Sensors & Diagnostics

PAPER

View Article Online
View Journal | View Issue



Cite this: *Sens. Diagn.*, 2026, **5**, 348

# Quantitative single-particle profiling of extracellular vesicles *via* fluorescent nanoparticle tracking analysis

Yiting Liu, [a] Anthony James El-Helou, [a] Bill Söderström, [b] Juanfang Ruan [c] and Ying Zhu *[adef]

Extracellular vesicles (EVs) have drawn rapidly increasing attention as the next-generation diagnostic biomarkers and therapeutic agents. However, the heterogeneous nature of EVs necessitates advanced methods for profiling EVs at the single-particle level. While nanoparticle tracking analysis (NTA) is a widely used technique for quantifying particle size and concentration, conventional scattering-based systems are non-specific. In this study, we present an optimised protocol for quantitative profiling of EVs at the single-particle level by fluorescent NTA (F-NTA). The protocol integrates fluorescent immunolabeling of EVs with size-exclusion chromatography (SEC) to efficiently remove unbound labels, enabling the precise quantification of EV concentration, size distribution, and surface immunophenotype. We first validated this approach using biotinylated liposomes and EVs from cultured human cell lines, confirming effective removal of unbound labels and assessing labelling efficiency. We then demonstrated that F-NTA can distinguish EV subpopulations with distinct surface marker expression, exemplified by the differentiation of EpCAM-positive (EpCAM$^+$) EVs derived from HT29 and HEK293 cells. Finally, we applied dual labelling to human plasma isolates to simultaneously profile EVs and lipoproteins, providing a quantitative quality assessment of EV purity at the single-particle level. The robustness of this method was further supported by comparative analysis with total internal reflection fluorescence microscopy. This validated workflow enables robust, quantitative profiling of EV subpopulations, providing a critical tool for diverse EV applications, including biomarker discovery, therapeutic monitoring, and quality control for engineered vesicles.

Received 4th July 2025,
Accepted 20th November 2025

DOI: 10.1039/d5sd00119f

rsc.li/sensors



## Introduction

Extracellular vesicles (EVs) are lipid bilayer-encapsulated micro- to nanoscale particles secreted by all cell types. EVs have drawn rapidly increasing attention as the next-generation diagnostic biomarkers and therapeutic agents, due to their critical roles in intercellular communication.[1–3] Their molecular cargo and surface markers, comprising proteins, lipids, and nucleic acids, can reflect the physiological or pathological state of the originating cells, making them especially valuable for non-invasive diagnostics. However, EVs are inherently heterogeneous, owing to diverse biogenesis pathways and cellular origins.[4] EVs derived from the same parent cell type can encompass multiple, distinct subpopulations. This complexity presents a major challenge for conventional bulk analytical methods such as Western blotting and enzyme-linked immunosorbent assay (ELISA), which lack the resolution to distinguish individual vesicle subtypes. Consequently, there is a critical need for single-EV analysis technologies capable of probing vesicles at the individual level, enabling more precise molecular characterisation and offering deeper insights into EV biology, function, and clinical potential.

The growing need for single-particle analysis of EVs has driven the development of a wide array of detection techniques and technologies.[5,6] Among the numerous single-EV analysis techniques, nanoparticle tracking analysis (NTA) remains the most widely adopted, due to its ability to simultaneously quantify size distribution and particle concentration, while also being widely accessible and easy to use through commercially available platforms. NTA employs optical tracking of Brownian motion to estimate hydrodynamic diameter *via* the Stokes–Einstein equation, while particle concentration is determined from scattering events detected at the single-particle level. Conventional NTA systems rely primarily on total light

[a] *School of Biomedical Engineering, University of Technology Sydney, Australia*
[b] *Australian Institute for Microbiology and Infection, University of Technology Sydney, Australia*
[c] *Electron Microscope Unit, UNSW Sydney, Australia*
[d] *School of Clinical Medicine, Faculty of Medicine & Health, UNSW Sydney, Australia. E-mail: ying.zhu@unsw.edu.au*
[e] *Institute for Biomedical Materials and Devices, University of Technology Sydney, Australia*
[f] *Australian Centre for NanoMedicine, UNSW Sydney, Australia*

scattering, rendering the measurements non-specific. This limitation compromises molecular discrimination and introduces ambiguity regarding the identity of detected particles, which may include co-isolated contaminants.

To overcome limitations in molecular discrimination, fluorescent NTA (F-NTA) has emerged as a key enhancement to conventional NTA. F-NTA builds on conventional scattering-based NTA by incorporating optical bandpass filters, enabling selective detection of fluorescently labelled particles. This advancement enables fluorescence-based phenotyping of EVs at the single-particle level, providing an approach to assess labelling strategies and molecular markers with enhanced specificity. Using F-NTA, Fortunato *et al.* systematically evaluated fluorescent labelling strategies for EVs, comparing lipid- and antibody-based dyes as well as washing protocols to minimize background signal from unbound dye.[7] In a comparative study of fluorescence quantification, Mladenović *et al.* found that F-NTA could detect as few as ~21 Alexa Fluor molecules, relative to nano-flow cytometry.[8] Moreover, Dlugolecka *et al.* provided one of the first demonstrations of F-NTA applied to patient-derived EVs, analysing bronchopulmonary lavage fluid and highlighting the challenges of measuring complex biofluids. This study underscores the technique's potential for clinical translation, while also revealing limitations in signal specificity and sample complexity.[9]

In this study, we present an optimised F-NTA protocol for profiling EVs with distinct surface phenotypes using fluorescent antibody labelling. While some studies have used ultracentrifugation to pellet EVs along with unbound fluorescent labels, this approach has been reported to exacerbate micelle formation, potentially confounding downstream fluorescence measurements.[10] To avoid micelle formation, we opted for size-exclusion chromatography (SEC), which has been reported to have the highest efficiency to remove unbound fluorescent labels compared with other washing methods.[11] Our previous work also showed that SEC achieves a good balance between EV yield and purity for plasma EV isolation.[12] F-NTA for measuring fluorescently labelled nanoparticles was first validated with biotinylated liposomes labelled with Alexa Fluor 488 (AF488) streptavidin, as well as EVs labelled with AF488 anti-CD63. Both F-NTA measurements yielded the expected labelling efficiency, determined by the proportion of fluorescent particles relative to the total particle count. We further applied F-NTA to differentiate between EVs carrying different levels of surface markers, demonstrated by measuring AF488 anti-EpCAM labelled EVs derived from HT29 and HEK293, which exhibit well-characterized differences in EpCAM expression from our previous work.[13] Finally, we demonstrated that F-NTA can profile distinct extracellular particle types within human plasma isolates by selectively labelling EVs with Alexa Fluor 647 (AF647) anti-CD63 and lipoproteins with AF488 anti-ApoB. This dual labelling strategy enabled single-particle assessment of EV isolation quality, which we further validated using total internal reflection fluorescence (TIRF) microscopy imaging.

# Experimental

## Materials

SEC qEV1 70 nm column and automatic fraction collector (AFC) V2 were purchased from Izon Science (USA). Non-PEGylated biotinylated liposomes (CDEIMS-1523), DiO-labelled liposomes (CDL6001F-DO) and DiD-labelled liposomes (CDL6001F-DD) were purchased from CD Bioparticles (USA). Lyophilised exosomes from HT29 (HBM-HT29-100/2) and HEK293 (HBM-HEK293-100/2) cell culture supernatant were purchased from HansaBiomed Life Sciences (Estonia). Very low-density lipoprotein (437647-5MG) was purchased from Merck Life Science (Germany). BD Vacutainer K2E EDTA tube (367525) was purchased from Becton Dickinson (UK). AF488 streptavidin conjugate (S11223) and AF488 anti-CD63 (MA5-18149) were purchased from Thermo Fisher Scientific (USA). AF488 anti-ApoB (sc-393636 AF488) was purchased from Santa Cruz (USA). Both AF488 anti-EpCAM (ab237395) and AF647 anti-CD63 (ab309976) were purchased from Abcam (UK). Phosphate-buffered saline (1× PBS) tablets, pH 7.2–7.6 (P4417) and poly-L-lysine (PLL) solution (P8920) were purchased from Sigma-Aldrich (USA). The Thermo-Shaker (TS-100C) was from Biosan (Latvia). Bottle-top vacuum 0.22 μm cellulose acetate filter system (CLS430517) was purchased from Corning (USA). Particle Metrix ZetaView PMX-420 QUATT and polystyrene (PS) 100 nm standard calibration beads were from Particle Metrix (Germany). High-precision coverslips no. 1.5, 25 × 75 mm (GVD7247) and sticky-Slide VI 0.4 (80608) for TIRF imaging were purchased from Knittel Glasbearbeitungs (Germany) and ibidi (Germany), respectively. The Nikon super-resolution microscope N-STORM was from Nikon (Japan). All antibody information used in this study is summarized in Table S1, and the reagents used are listed in Table S2.

## Human blood collection and plasma extraction

Human blood samples were collected in accordance with the National Statement on Ethical Conduct in Human Research 2023, under the University of Technology Sydney Human Research Ethics Committees Approval ETH21-5782. Informed consent was obtained from the human participants in this study. 10 mL of human blood was collected from the Australian Red Cross (Life Blood Sydney, NSW, Australia) using ethylenediaminetetraacetic acid (EDTA) tubes. Plasma was extracted by a two-step centrifugation according to a previous methodological guideline to reduce platelet-derived EVs.[14] Briefly, the whole blood was first centrifuged at 2500 × *g* for 15 minutes at room temperature. The supernatant was gently transferred to a new 15 mL tube and centrifuged again at 2500 × *g* for 15 minutes at room temperature. The collected plasma was aliquoted into 1 mL and stored at −80 °C before use.

## Size-exclusion chromatography (SEC) for unbound label removal and plasma EV isolation

The qEV1 70 column was loaded in AFC to isolate EV and used based on the manufacturer's instructions. All the runs

were performed at room temperature. In general, the column was first washed with 27 mL particle-free 1× PBS before sample loading. The sample was topped up to 1 mL particle-free 1× PBS for column loading if the original volume was below 1 mL. A total volume of 2.8 mL was collected after the buffer volume for each SEC run. All fractions were obtained in elution with particle-free 1× PBS. After every SEC round, the column was washed with 13.5 mL 0.5 M NaOH, followed by washing with 27 mL of 1× PBS. For future use, the column was stored in 20% ethanol until the next run.

Following isolation, the EVs were fluorescently labelled to enable downstream detection, and the same qEV1 70 nm column was used for both purposes of unbound label removal and plasma EV isolation, with slightly different buffer volumes based on the manufacturer's user manual and recommendations. For unbound label removal, the buffer volume was set to 4 mL, so that the sample was collected from 4.0–6.8 mL to maximise the EV recovery. For plasma EV isolation, the default buffer volume of 4.7 mL was used, and the samples were collected from 4.7–7.5 mL to maximise the EV purity.

### Fluorescence labelling of EVs, lipoproteins and liposomes

EVs, lipoproteins and liposomes were labelled with fluorescent antibodies or proteins according to the conditions in Table 1. Specifically, the sample and fluorescence label were mixed according to the concentrations and volumes listed in Table 1 and incubated for 2 hours at room temperature in the dark on the thermo-shaker at a constant low speed (250 rpm). All necessary dilutions were performed with 0.22 μm filtered particle-free 1× PBS. To quantify both the total and fluorescently labelled particle populations, we next performed NTA.

### Nanoparticle tracking analysis (NTA)

Particle concentration and size distribution were measured by ZetaView PMX-420 QUATT in scatter and fluorescence modes with software version 8.05.16_SP3. The instrument was auto-aligned with the 100 nm PS standard beads before sample measurement. Before each sample injection, the flow cell was flushed with fresh Milli-Q water and then primed with fresh PBS to avoid turbulent drift. Samples were diluted with particle-free 1× PBS to reach the optimal particle concentration within the manufacturer-recommended measurement range (approximately $5 \times 10^6$ to $1 \times 10^8$ particles per mL).

The detailed parameters for scattering and fluorescent NTA measurements are listed in Table 2. The default laser wavelength for scattering measurement was 488 nm. For fluorescence measurement, laser/filter wavelength combinations 488/500 nm and 640/660 nm were used for AF488 and AF647 antibodies, respectively. All fluorescence measurements were conducted under the "low bleach" mode to minimise photobleaching during data acquisition. In case of multiple measurements of a single sample, the "Multiple Acquisitions" and "dose sub volume" modes were used to enhance the statistics of the replicate measurements. For each measurement, 11 different positions across different focal planes of the flow cells were measured, generating 11 replicates for the particle concentration and size distribution data, including median and mode sizes. For size distribution, a bin size of 10 nm was used for the histogram display.

For each fluorescent measurement, commercial fluorescent liposomes that matched the specific laser/filter wavelengths were used as the fluorescence standards to obtain the concentration correction factor. DiO liposomes were used for 488/500 nm, and DiD liposomes were used for 640/660 nm. Briefly, the fluorescence standards were measured first in both scattering and fluorescence modes. A number of particles *vs.* sensitivity (NvS) graph was generated to plot the relationship between sensitivity and the number of particles detected in the field of view. The concentration correction factor ($K_f$) was determined by the following equation:

$$K_f = \frac{n_{det}(S, \text{sens} = 80)}{n_{det}(F, \text{sens} = 95)}$$

where $n_{det}(S, \text{sens} = 80)$ is the number of particles detected in scatter mode at a sensitivity of 80, and $n_{det}(F, \text{sens} = 95)$ is the number of particles detected in fluorescent mode at a sensitivity of 95. All fluorescence concentrations were then multiplied by the $K_f$ to obtain the corrected concentration values.

### Total internal reflection fluorescence (TIRF) microscopy imaging and data processing

The fluorescently labelled human plasma isolation sample was immobilised onto a coverslip for TIRF microscopy

Table 1 Summary of fluorescence labelling conditions for liposomes, lipoproteins and EVs

| Sample | Sample vol. (μL) | Particle concentration[a] (/mL) | Fluorescence label | Label vol. (μL) | Label vol. (mg mL$^{-1}$) |
|---|---|---|---|---|---|
| Biotin-liposome | 100 | $1.6 \times 10^9$ | AF488 streptavidin | 5 | 0.5 |
| Lipoprotein | 100 | $2.2 \times 10^{10}$ | AF488 anti-ApoB | 10 | 0.2 |
| HT29 | 100 | $6.6 \times 10^{10}$ | AF488 anti-CD63 | 10 | 0.26 |
| HT29 | 100 | $6.6 \times 10^{10}$ | AF647 anti-CD63 | 10 | 0.25 |
| HT29 | 100 | $6.6 \times 10^{10}$ | AF488 anti-EpCAM | 10 | 0.25 |
| HEK293 | 100 | $1.8 \times 10^{10}$ | AF488 anti-EpCAM | 10 | 0.25 |
| Human plasma isolate | 200 | $6.2 \times 10^{10}$ | AF647 anti-CD63 | 20 | 0.25 |
| | | | AF488 anti-ApoB | 20 | 0.2 |

[a] The particle concentration was measured by scattering NTA measurement.

Table 2 The detailed parameters for scattering and fluorescent NTA measurements

| | Pre-acquisition parameter | | | | Post-acquisition parameter | | | |
|---|---|---|---|---|---|---|---|---|
| Type | Camera sensitivity | Camera shutter | Number of frames | Frame rate | Minimum brightness | Min area | Max area | Trace length |
| Scattering (S-NTA) | 80 | 100 | High | 30 | 30 | 10 | 1000 | 15 |
| Fluorescent (F-NTA) | 95 | 100 | Low | 30 | 30 | 10 | 1000 | 7 |

imaging. A coverslip was cleaned with $O_2$ plasma for 1 minute, incubated with 1 mg $mL^{-1}$ poly-L-lysine (PLL), rinsed with Milli-Q water, and blow-dried. The PLL-coated coverslip was assembled with a 6-channel sticky slide cartridge (sticky-Slide VI 0.4, ibidi). A 30 μL sample was introduced to the cartridge channel and incubated in the dark for 1 hour, which allows the electrostatic adsorption of the negatively charged particles (EVs and lipoproteins) to the positively charged coverslip. Then, the channel was rinsed with 120 μL of 1× PBS. After washing, 60 μL of 1× PBS was added to each reservoir, and the cartridge was transferred to the microscope for imaging.

Fluorescence images were acquired on a Nikon TiE2 N-STORM microscopy equipped with a sCMOS camera and a CFI HP Plan Apochromat VC 100× oil immersion objective, operated in TIRF mode. Low laser power of 5% and an exposure time of 400 ms were used for both 488 nm and 647 nm laser filter settings. The Perfect Focus System (PFS) was activated to maintain the samples in focus throughout the image acquisition time. The region of interest (ROI) was set to 1024 × 1024 pixels (0.065 μm per pixel). To ensure representative sampling while minimising photobleaching, images were captured at eight distinct locations spaced from one side of the channel to the other.

The fluorescence images were subsequently analysed using Fiji ImageJ. The open-source plugin, EVAnalyzer, was used for automatic quantification of EV numbers in each image.[15] The EVAnalyzer processes all images in the chosen input folder with the same settings and saves the results in a default, automatically created output folder. For a single experiment, all samples and controls were analysed with consistent settings. The specific parameter settings are as follows: Series to import: Series_1 (488 nm channel) and Series_2 (647 nm channel); function: EV counts, type: EV_GPF and EV_CY5; threshold algorithm: manual; manual threshold: 100; min circularity: 0. The image analysis results consist of a report file in .xlsx format, output images, and a .json file, which includes all settings and can be used to reload the configuration.

### Data analysis

All data were analysed and visualised using GraphPad Prism (version 10.4.2). Bar charts were presented as mean (solid bar) ± standard deviation (vertical error bar). The violin plots were presented with medium smoothing. The median value of each group is indicated by a dashed line within the plot. Statistical comparisons between two groups were performed using an unpaired two-tailed *t*-test. *P* values were considered statistically significant as follows: ≤0.05 (*), ≤0.01 (**), ≤0.001 (***), ≤0.0001 (****).

For the initial validation experiments (Fig. 2 and 3), the SEC eluate (4.0–6.8 mL) was collected as four separate 0.7 mL fractions. Each fraction was measured once, generating data from 11 positions within the NTA flow cell. As no consistent trend was observed between the individual fractions, the data from all four fractions were pooled for analysis, resulting in a total of $n$ = 44 technical replicates. For subsequent experiments (Fig. 4 and 5), the entire 4.0–6.8 mL eluate was pooled first, and this single sample was measured in triplicate. With each measurement comprising 11 positions, this resulted in a total of $n$ = 33 technical replicates.

## Results and discussion

Our F-NTA workflow enables efficient fluorescent profiling of EVs through a streamlined process integrating plasma-derived EV isolation, antibody-based labelling, removal of unbound fluorophores, and single-particle quantification (Fig. 1). After isolation, EVs or other investigated particles, such as lipoproteins and liposomes, were first fluorescently labelled and then purified by SEC. In this step, the flow of smaller particles along the column is slower than that of larger particles, as they tend to be trapped by the porous resin, resulting in size-based particle separation. Labelled EVs or other particles were collected during the earlier stages of elution, leaving the unbound antibody or protein labels in the later stages. The early elution fractions (4.0–6.8 mL) were collected according to the manufacturer's guidelines to maximise EV recovery (see experimental for details). This workflow provided a consistent source of labelled EVs for downstream quantification and ensured that subsequent analyses reflected the EV population rather than free fluorescent labels.

After removing unbound labels, purified EVs were measured using NTA on the ZetaView PMX-420 system (Particle Metrix), which detects total particle counts *via* scattered light and fluorescently labelled particles *via* fluorescence emission. In samples with 100% fluorescent particles, the particle count measured in scattering NTA (S-NTA) is typically higher than that measured in F-NTA. This discrepancy arises because weakly fluorescent particles may fall below the detection threshold, as the emitted light must pass through a filter before reaching the camera. To compensate for this loss, we used a higher sensitivity (95) in fluorescence mode compared to scattering

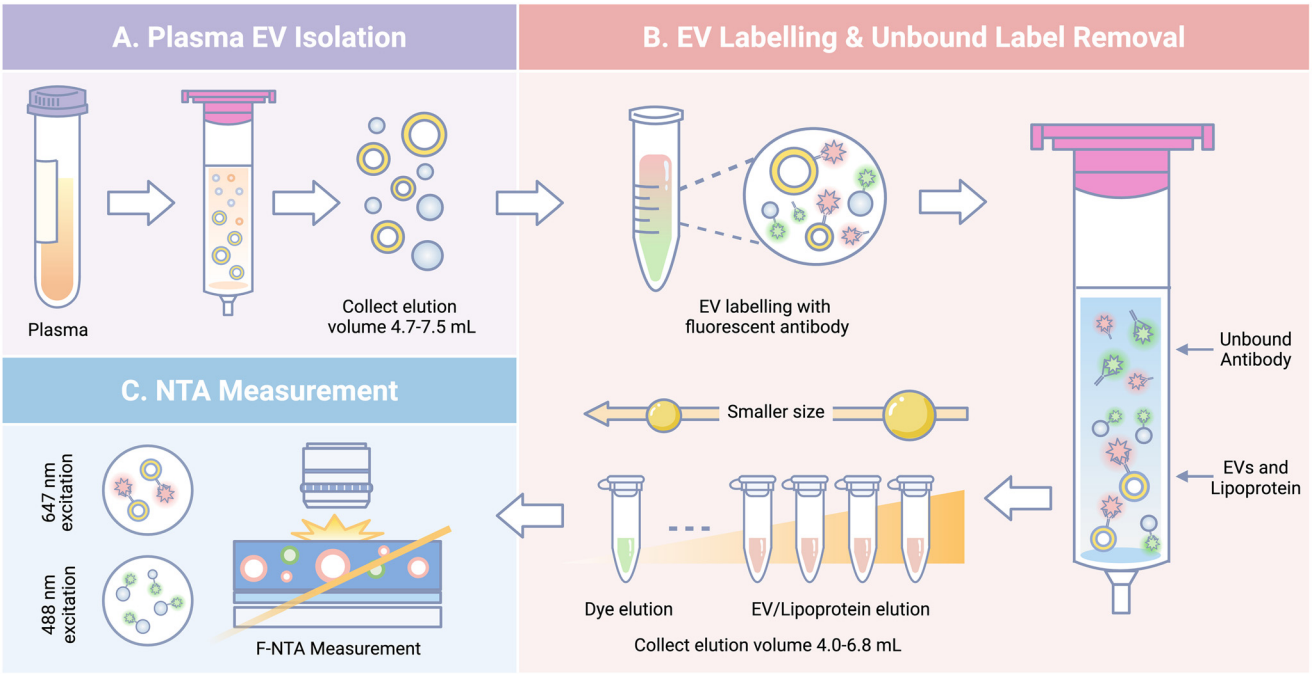


**Fig. 1** Schematic diagram of the whole F-NTA workflow. A) Plasma EVs are isolated using the SEC column. The elute volume of 4.7–7.5 mL is collected to maximise the EV purity. B) EVs and other investigated particles, like lipoproteins and liposomes, are labelled in solution with fluorescent antibodies or proteins. Different fluorescent dyes, including AF488 (green) and AF647 (pink), are used for multiplexed detection. To remove excess unbound labels, the labelled samples were further processed through the same SEC column but collected at a different elution volume of 4.0–6.8 mL to maximise the EV recovery. C) F-NTA is then used to measure fluorescently labelled particles.

mode (80) and applied a $K_f$ to correct the fluorescent particle count (see experimental for details). The $K_f$ was obtained by measuring fluorescent liposomes, which have a similar lipid bilayer structure and refractive index (RI ~1.36–1.39) to EVs (RI ~1.37–1.39) and thus serve as a more accurate reference material compared to solid nanoparticles, such as fluorescent polystyrene beads.[16] The fluorescent liposomes were formed by incorporating lipophilic dyes (DiO, DiD *etc.*) into the lipid bilayers during production, and thus can be considered 100% fluorescent particles.

### SEC effectively removes unbound fluorescence labels

A key challenge in F-NTA measurements is the interference from unbound fluorescent labels, which can generate false-positive signals and elevate background noise, thereby obscuring weakly fluorescent particles. This issue is exacerbated for EVs due to their low density, which makes it difficult to separate them from excess fluorescence labels. To address this, we investigated the efficacy of SEC to remove excess unbound dye. As shown in Fig. 2, SEC effectively removes unbound fluorescence labels, demonstrated by comparing antibody solutions of equal concentration before and after SEC label removal. Fig. 2A depicts a representative field of view image of AF488 anti-ApoB, before and after SEC label removal. A dramatic reduction in fluorescent intensity was observed after the label removal process. This background suppression enabled the reliable measurement of fluorescently labelled EVs and other investigated particles, which would otherwise be undetectable due to high background signal from unbound fluorophores.

To evaluate the influence of elevated background signals from unbound labels, we quantified fluorescent particle counts in both SEC-removed and unremoved samples, using EVs derived from the human colon adenocarcinoma cell line HT29 (HT29 EVs) as a representative model. Fig. 2B shows the results from HT29 EVs labelled with AF488 anti-CD63, compared with the same volume of solution of anti-CD63. The unremoved labels accounted for only 4.22% of the total fluorescent particles, which were considered negligible for our subsequent investigations. We also investigated very low-density lipoprotein (VLDL) from human plasma, which is a predominant type of particle from human plasma that co-isolates with EVs.[12] The VLDL was labelled with AF488 anti-ApoB and was investigated with the same comparison as HT29 EVs. Fig. 2C shows comparable results to Fig. 2B, in which the unremoved labels account for only 8.66% of the total fluorescent particles, demonstrating the versatility of the SEC process in removing different fluorescence antibody labels.

### Validate particle labelling efficiency with fluorescent proteins and antibodies

Next, we validated the fluorescent labelling efficiency of our proposed F-NTA workflow using liposomes and EVs after SEC unbound label removal. The labelling efficiency was calculated

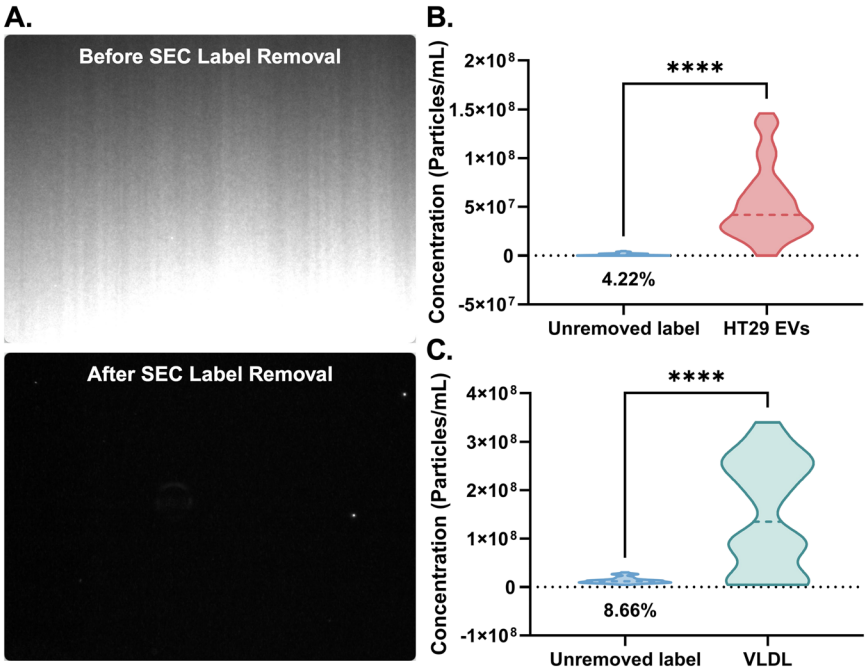


**Fig. 2** Performance of the SEC label removal. A) Representative screenshots from the ZetaView PMX-420 QUATT, equipped with a high-sensitivity CMOS camera (1920 × 1080 pixels), show recorded videos before (top) and after (bottom) SEC label removal using AF488 anti-ApoB for demonstration. High background noise is observed in the original fluorescence antibody solution, which drops dramatically after the SEC label removal. B and C) Comparison of the particle concentrations of labelled HT29 EV (B) and VLDL (C) and their corresponding free labels after SEC label removal. The proportion of unremoved labels out of the total fluorescent particles is 4.22% for HT29 EVs and 8.66% for VLDL, which are considered negligible ($p < 0.0001$). The data are from $n$ = 44, which includes a sum of four fractions (0.7 mL each) that were collected from the elute volume 4.0–6.8 mL and measured separately. Each sample was measured at 11 positions (see experimental section for details). The median value of each group is represented as a dashed line.

as the ratio of the corrected fluorescent particle concentration ($C_{F\text{-}NTA}$) to the total scatter particle concentration ($C_{S\text{-}NTA}$), using the following equation:

$$\text{Labelling efficiency } (\%) = \frac{C_{F\text{-}NTA} \times K_f}{C_{S\text{-}NTA}} \times 100$$

We initially utilise biotinylated liposomes labelled with AF488 streptavidin, leveraging the high affinity and stability of the biotin–streptavidin interaction. Fig. 3A demonstrates a labelling efficiency as high as 63.2%. Size comparison revealed no significant difference between the scatter and fluorescent modes. However, the size distribution obtained from F-NTA appears broader than that for S-NTA (Fig. 3B). The broader size distribution observed in F-NTA may be attributed to heterogeneous labelling efficiency among EV subpopulations, which leads to variations in fluorescence intensity and consequently, in the calculated particle size distribution. Furthermore, a shorter minimum trace length, defined as the minimum number of consecutive frames in which a particle must be tracked for inclusion in the analysis, was implemented for F-NTA measurements to reduce photobleaching. This adjustment introduced greater statistical uncertainty in particle size estimation. Labelling HT29-derived EVs with AF488-conjugated anti-CD63 antibodies resulted in 8.09% of the total particles exhibiting detectable fluorescence, reflecting the effective labelling efficiency under the given experimental conditions (Fig. 3C). This proportion is considered acceptable given that only CD63 was targeted, and not all EVs within the heterogeneous population are expected to express this single marker.[17] Furthermore, this percentage is comparable to that reported previously in similar work undertaken by Mladenović *et al.*, which was approximately 2%.[8] Notably, cryo-electron microscopy of the commercially sourced HT29 EVs revealed the presence of non-vesicular extracellular particles (NVEPs) alongside vesicular structures (Fig. S1). This indicates that the fluorescent particle percentage measured by F-NTA is an underestimation of the labelling efficiency between anti-CD63 and $CD63^+$ EVs, as the total particle number by S-NTA also contains NVEPs. Size comparison revealed a modest increase in average particle diameter from 114.9 nm to 133.1 nm (Fig. 3D). This shift reflects the added hydrodynamic size from antibody labelling, which typically contributes 10–15 nm and thus increases the apparent particle size measured by NTA. This conclusion is consistent with previous observations by Fortunato *et al.* and Bao *et al.*[7,18]

### F-NTA can differentiate between EVs carrying different levels of surface markers

To evaluate the biomarker profiling capability of F-NTA, we examined its ability to distinguish EV subpopulations based on

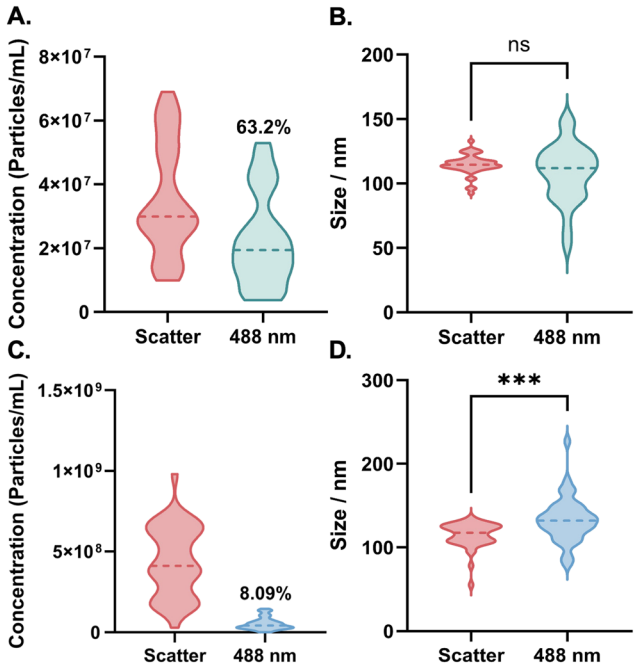


**Fig. 3** Particle labelling efficiency. A) Concentration and B) size analysis of AF488 streptavidin labelled liposomes measured in scatter (red) and fluorescent (green) modes. The proportion of fluorescent particles in total particles is 63.2%. A size comparison reveals no significant difference ($p$ = 0.0859) between the scatter and fluorescent modes. C) Concentration and D) size analysis of AF488 anti-CD63 labelled HT29 EVs measured in scatter (red) and fluorescent (blue) modes. The proportion of fluorescent particles in total particles is 8.09%. Size comparison shows a slight increase in the average size from 114.9 nm to 133.1 nm ($p$ = 0.0002). The data are from $n$ = 44, which includes a sum of four fractions (0.7 mL each) collected from the elute volume of 4.0–6.8 mL and measured separately. Each sample was measured at 11 positions (see experimental section for details). The median value of each group is represented as a dashed line.

surface marker expression. Our previous study demonstrated that HT29 EVs contain a significantly higher proportion of EpCAM-positive ($EpCAM^+$) EVs compared to the human embryonic kidney cell line HEK293 (HEK293 EVs), providing well-defined comparison samples for validating F-NTA's capability for biomarker profiling.[13] HT29 and HEK293 EVs were labelled with AF488 anti-EpCAM and measured by F-NTA after SEC label removal. Fig. 4A presents the particle concentrations from S-NTA and F-NTA for both EVs, and Fig. 4B shows the corresponding fluorescent particle proportion comparison. The results clearly show that HT29 EVs carry a significantly higher proportion of $EpCAM^+$ EVs (61.63%) compared to HEK293 EVs (19.43%). This result also highlights that, unlike bulk analysis methods such as Western blotting or ELISA, single EV analysis techniques like F-NTA do not require sample loading normalization or calibration curves. Biomarker differences can be quantified directly from the ratio of fluorescent to total particles. Size distribution measurements indicate that both EV populations retain a normal distribution after fluorescence labelling. While no significant change in size distribution was observed for HT29 EVs before and after labelling (Fig. 4C), HEK293 EVs exhibited a shift toward smaller particle sizes following labelling (Fig. 4D). This shift may be attributed to the low abundance of fluorescently labelled HEK293 EVs, which limits the ability to obtain a statistically robust size distribution.

### F-NTA can be used to assess the purity of EVs isolated from complex samples

EV purity is a critical parameter in evaluating the quality of EV isolation. Achieving high EV purity is particularly challenging in complex biological matrices such as human plasma. In our previous study, we established a bulk method to assess EV quality using immunomagnetic beads for EV capturing, followed by flow cytometry analysis.[12] In contrast, this study investigates whether F-NTA can be applied for quality assessment of plasma-derived EVs at the single-particle level. For plasma EV isolation, the same SEC column used for unbound label removal was employed, but with an adjusted elution volume of 4.7–7.5 mL to maximise EV purity (see experimental section for details). Cryo-electron microscopy images confirmed the presence of EVs in the isolates (Fig. S2). Lipoproteins were used to assess impurity in plasma EV isolation, as they are the predominant contaminants and vastly outnumber EVs in human plasma.[19] While SEC is effective in removing the majority of high-density lipoproteins (HDL), it cannot remove other types, such as VLDL and chylomicrons, sufficiently, which have similar densities and sizes to EVs.[20] ApoB marker has been reported to reliably recognise lipoproteins, including VLDL and chylomicrons.[21] Therefore, in this study, the isolates were labelled with two fluorescent antibodies with different fluorescent dyes, AF647 anti-CD63 for EV labelling, and AF488 anti-ApoB for lipoprotein labelling. F-NTA measurements revealed the presence of both EVs and lipoproteins. As shown in Fig. 5A, lipoproteins exhibited significantly higher concentrations than EVs across the interrogated size range. Based on F-NTA quantification, the EV-to-lipoprotein ratio was 7.44% (Fig. 5C). We compared the results obtained by F-NTA with another single EV technique, using TIRF microscopy imaging. The same sample, measured by F-NTA, was introduced onto a PLL-coated microscopy coverslip through the electrostatic absorption of EVs and lipoproteins, and then imaged by a fluorescence microscope using TIRF illumination. Fig. 5B shows the presence of anti-CD63 labelled EVs (pink dots) and anti-ApoB labelled lipoproteins (green dots) in the same field of view. A quantitative analysis of the image shows an EV : lipoprotein ratio of 27.92%. This difference in quantification can be attributed to the distinct detection principles of the two methods. F-NTA is a dynamic technique that analyses particles freely diffusing in solution. For a particle to be counted, it must produce a fluorescent signal bright enough to exceed the detection threshold within the short exposure time of a single video frame. This makes F-NTA a powerful tool for characterising particle size and concentration in solution, but sets a stringent requirement for signal intensity. In contrast,

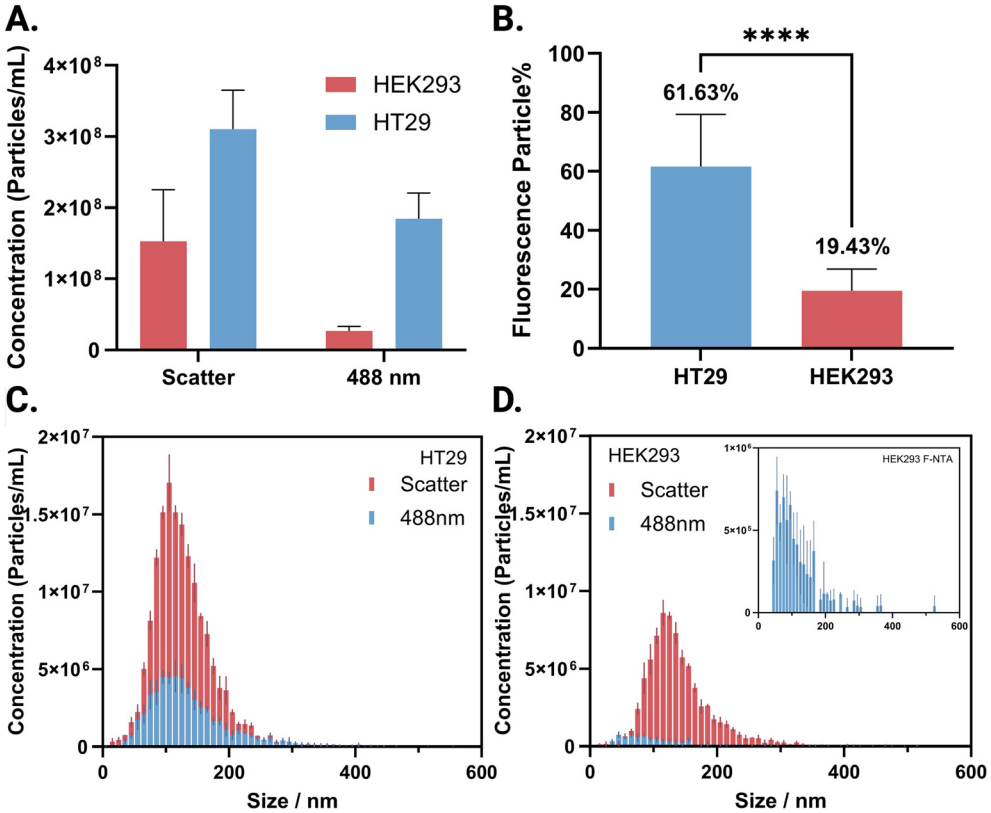


**Fig. 4** Comparison of EpCAM$^+$ EVs between HT29 and HEK293 EVs. A) Total particle concentrations from S-NTA (scatter) and fluorescent particle concentration from F-NTA (488 nm). B) Comparison of EpCAM$^+$ EVs, as shown by the proportion of fluorescent particles. HT29 EVs (61.63%) showed a significantly higher proportion ($p < 0.0001$) compared to HEK293 EVs (19.43%), consistent with the different EpCAM expression of the EVs from the two cell lines. The data are from $n = 33$, which includes three measurements of a sample at 11 positions from the total collected volume 4.0–6.8 mL (see experimental section for details). (C and D) Corresponding size distributions from (C) HT29 EVs and (D) HEK293 EVs in scatter (red) and fluorescent (blue) modes. The size distribution histograms are presented as mean (solid bar) ± standard deviation (vertical error bar).

TIRF microscopy is a static method that analyses particles immobilised on a surface. This allows for the use of longer exposure times, enabling the accumulation of photons from even dimly labelled particles. While this approach offers high sensitivity for enumerating surface-captured fluorophores, it does not provide the in-solution hydrodynamic size and concentration data that F-NTA does. These fundamental differences in particle state (dynamic *vs.* static) and signal acquisition logically result in the observed quantitative discrepancies.

## Conclusions

In this study, we established an optimised protocol for quantitative single-particle profiling that integrates fluorescent antibody labelling, SEC label removal and F-NTA. This robust workflow enables reliable quantification of surface marker expression and the accurate assessment of EV purity in a single, integrated approach. Looking forward, the capabilities of F-NTA can be further expanded. Future advancements, such as improving camera sensitivity, using next-generation ultra-bright fluorophores and nanoprobes, and implementing advanced analytical software, will continue to improve the detection limit for dimly labelled and rare EV populations. Furthermore, this workflow provides a foundation for multiplexed co-localisation analysis using next-generation NTA instruments. Ultimately, this work provides the research community with a critical and accessible tool for developing EV-based diagnostics, monitoring therapeutic efficacy, and performing quality control on engineered vesicles for drug delivery.

## Author contributions

YL: conceptualisation, data curation, formal analysis, investigation, methodology, validation, visualisation, writing – original draft; AJE: formal analysis, writing – review & editing; BS: resources, supervision, writing – review & editing; JR: investigation, writing – review & editing; YZ: conceptualisation, formal analysis, funding acquisition, methodology, project administration, writing – original draft.

## Conflicts of interest

The authors declare no conflicts of interest in this work.

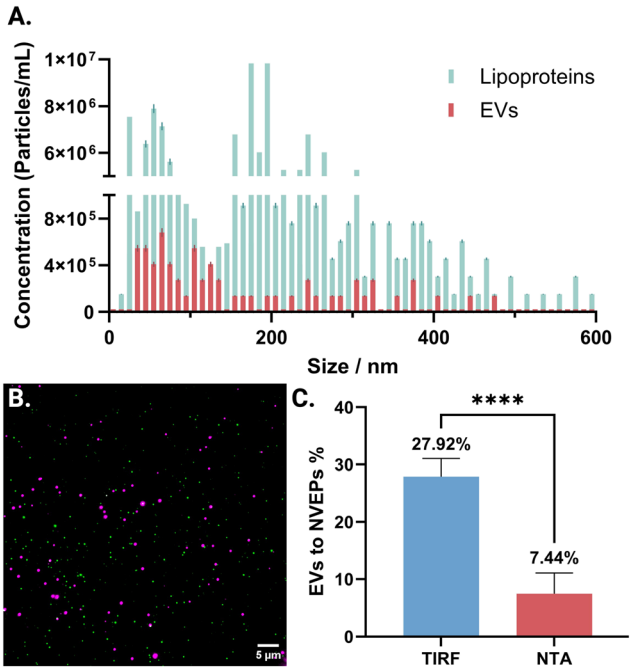


**Fig. 5** A) Concentration distribution of EVs and lipoproteins measured by F-NTA across particle sizes ranging from 5 to 600 nm. The histograms are presented as mean (solid bar) ± standard deviation (vertical error bar). B) Representative TIRF image of labelled EVs (magenta) and lipoproteins (green). Scale bar: 5 μm. C) Quantitative comparison of EV-to-lipoprotein detected by TIRF and F-NTA. TIRF analysis revealed a significantly higher ($p < 0.0001$) EV-to-lipoprotein ratio (27.92%) compared to F-NTA (7.44%). The data from TIRF are from $n$ = 8, obtained from eight different imaging locations across the microfluidic channel. NTA data are from $n$ = 33, which includes three measurements of a sample at 11 positions from the total collected volume 4.0–6.8 mL.

## Data availability

The datasets supporting this article have been uploaded as part of the supplementary information (SI). Further information relevant to this study is available from the authors upon request. We have submitted all relevant data of our experiments to the EV-TRACK knowledge base (EV-TRACK ID: EV250078). Supplementary information: includes tables of antibodies and reagents used in this study and Cryo-EM images. See DOI: https://doi.org/10.1039/d5sd00119f.

## Acknowledgements

We acknowledge the following funding support: the Australian Research Council Discovery Early Career Researcher Awards (DE240100321) for Y. Z. and the Australian Research Council Future Fellowship (FT230100062) for B. S.; PanKind, The Australian Pancreatic Cancer Foundation (24. R10.EDG.YZ.UTSY) for Y. Z. We thank Dr Sven Kreutel from Particle Metrix for his technical support. We also thank Dr Yunyun Hu and Professor Xiaomei Yan from Xiamen University for their discussions regarding antibody dye removal and EV labelling.

## References

1 R. Kalluri and V. S. LeBleu, The biology, function, and biomedical applications of exosomes, *Science*, 2020, **367**, eaau6977.
2 R. Kalluri and K. M. McAndrews, The role of extracellular vesicles in cancer, *Cell*, 2023, **186**, 1610–1626.
3 I. K. Herrmann, M. J. A. Wood and G. Fuhrmann, Extracellular vesicles as a next-generation drug delivery platform, *Nat. Nanotechnol.*, 2021, **16**, 748–759.
4 R. P. Carney, R. R. Mizenko, B. T. Bozkurt, N. Lowe, T. Henson, A. Arizzi, A. Wang, C. Tan and S. C. George, Harnessing extracellular vesicle heterogeneity for diagnostic and therapeutic applications, *Nat. Nanotechnol.*, 2025, **20**, 14–25.
5 G. Bordanaba-Florit, F. Royo, S. G. Kruglik and J. M. Falcón-Pérez, Using single-vesicle technologies to unravel the heterogeneity of extracellular vesicles, *Nat. Protoc.*, 2021, **16**, 3163–3185.
6 T. Wang, Y. Xing, Z. Cheng and F. Yu, Analysis of single extracellular vesicles for biomedical applications with especial emphasis on cancer investigations, *TrAC, Trends Anal. Chem.*, 2022, **152**, 116604.
7 D. Fortunato, D. Mladenović, M. Criscuoli, F. Loria, K.-L. Veiman, D. Zocco, K. Koort and N. Zarovni, Opportunities and Pitfalls of Fluorescent Labeling Methodologies for Extracellular Vesicle Profiling on High-Resolution Single-Particle Platforms, *Int. J. Mol. Sci.*, 2021, **22**, 10510.
8 D. Mladenović, J. Brealey, B. Peacock, K. Koort and N. Zarovni, Quantitative fluorescent nanoparticle tracking analysis and nano-flow cytometry enable advanced characterization of single extracellular vesicles, *J. Extracell. Biol.*, 2025, **4**, e70031.
9 M. Dlugolecka, J. Szymanski, L. Zareba, Z. Homoncik, J. Domagala-Kulawik, M. Polubiec-Kownacka and M. Czystowska-Kuzmicz, Characterization of Extracellular Vesicles from Bronchoalveolar Lavage Fluid and Plasma of Patients with Lung Lesions Using Fluorescence Nanoparticle Tracking Analysis, *Cell*, 2021, **10**, 3473.
10 P. Pužar Dominkuš, M. Stenovec, S. Sitar, E. Lasič, R. Zorec, A. Plemenitaš, E. Žagar, M. Kreft and M. Lenassi, PKH26 labeling of extracellular vesicles: Characterization and cellular internalization of contaminating PKH26 nanoparticles, *Biochim. Biophys. Acta, Biomembr.*, 2018, **1860**, 1350–1361.
11 H. Kobayashi, T. Shiba, T. Yoshida, D. Bolidong, K. Kato, Y. Sato, M. Mochizuki, T. Seto, S. Kawashiri and R. Hanayama, Precise analysis of single small extracellular vesicles using flow cytometry, *Sci. Rep.*, 2024, **14**, 7465.
12 B. Pang, Y. Zhu, J. Ni, J. Ruan, J. Thompson, D. Malouf, J. Bucci, P. Graham and Y. Li, Quality assessment and comparison of plasma-derived extracellular vesicles separated by three commercial kits for prostate cancer diagnosis, *Int. J. Nanomed.*, 2020, 10241–10256.
13 G. Huang, Y. Zhu, S. Wen, H. Mei, Y. Liu, D. Wang, M. Maddahfar, Q. P. Su, G. Lin, Y. Chen and D. Jin, Single Small Extracellular Vesicle (sEV) Quantification by Upconversion Nanoparticles, *Nano Lett.*, 2022, **22**, 3761–3769.

14 F. A. W. Coumans, A. R. Brisson, E. I. Buzas, F. Dignat-George, E. E. E. Drees, S. El-Andaloussi, C. Emanueli, A. Gasecka, A. Hendrix, A. F. Hill, R. Lacroix, Y. Lee, T. G. van Leeuwen, N. Mackman, I. Mäger, J. P. Nolan, E. van der Pol, D. M. Pegtel, S. Sahoo, P. R. M. Siljander, G. Sturk, O. de Wever and R. Nieuwland, Methodological Guidelines to Study Extracellular Vesicles, *Circ. Res.*, 2017, **120**, 1632–1648.

15 M. Schürz, J. Danmayr, M. Jaritsch, E. Klinglmayr, H. M. Benirschke, C.-T. Matea, P. Zimmerebner, J. Rauter, M. Wolf, F. G. Gomes, Z. Kratochvil, Z. Heger, A. Miller, T. Heuser, V. Stanojlovic, J. Kiefer, T. Plank, L. Johnson, M. Himly, C. Blöchl, C. G. Huber, M. Hintersteiner and N. Meisner-Kober, EVAnalyzer: High content imaging for rigorous characterisation of single extracellular vesicles using standard laboratory equipment and a new open-source ImageJ/Fiji plugin, *J. Extracell. Vesicles*, 2022, **11**, 12282.

16 C. Gardiner, M. Shaw, P. Hole, J. Smith, D. Tannetta, C. W. Redman and I. L. Sargent, Measurement of refractive index by nanoparticle tracking analysis reveals heterogeneity in extracellular vesicles, *J. Extracell. Vesicles*, 2014, **3**, 25361.

17 R. R. Mizenko, T. Brostoff, T. Rojalin, H. J. Koster, H. S. Swindell, G. S. Leiserowitz, A. Wang and R. P. Carney, Tetraspanins are unevenly distributed across single extracellular vesicles and bias sensitivity to multiplexed cancer biomarkers, *J. Nanobiotechnol.*, 2021, **19**, 250.

18 C. Bao, H. Xiang, Q. Chen, Y. Zhao, Q. Gao, F. Huang and L. Mao, A Review of Labeling Approaches Used in Small Extracellular Vesicles Tracing and Imaging, *Int. J. Nanomed.*, 2023, **18**, 4567–4588.

19 J. B. Simonsen, What Are We Looking At? Extracellular Vesicles, Lipoproteins, or Both?, *Circ. Res.*, 2017, **121**, 920–922.

20 A. N. Böing, E. van der Pol, A. E. Grootemaat, F. A. W. Coumans, A. Sturk and R. Nieuwland, Single-step isolation of extracellular vesicles by size-exclusion chromatography, *J. Extracell. Vesicles*, 2014, **3**, 23430.

21 B. W. Sódar, Á. Kittel, K. Pálóczi, K. V. Vukman, X. Osteikoetxea, K. Szabó-Taylor, A. Németh, B. Sperlágh, T. Baranyai, Z. Giricz, Z. Wiener, L. Turiák, L. Drahos, É. Pállinger, K. Vékey, P. Ferdinandy, A. Falus and E. I. Buzás, Low-density lipoprotein mimics blood plasma-derived exosomes and microvesicles during isolation and detection, *Sci. Rep.*, 2016, **6**, 24316.